

Article

Hydrothermally Synthesized Hydroxyapatite-Silica Composites with Enhanced Mechanical Properties for Bone Graft Applications

Atiek Rostika Noviyanti ^{1,*}, Juliandri Juliandri ¹, Engela Evy Ernawati ¹, Haryono Haryono ¹, Solihudin Solihudin ¹, Dina Dwiyantri ¹, Azman Ma'amor ², Ferli Septi Irwansyah ^{1,3,*} and Sharifuddin Bin Md Zain ²

¹ Departement of Chemistry, Faculty of Mathematics and Natural Sciences, Universitas Padjadjaran, Sumedang 45363, Indonesia; juliandri@unpad.ac.id (J.J.); ernawati@unpad.ac.id (E.E.E.); haryono@unpad.ac.id (H.H.); solihudin@unpad.ac.id (S.S.); dina.dwiyantri@unpad.ac.id (D.D.)

² Departement of Chemistry, Faculty of Science, University of Malaya, Kuala Lumpur 56000, Malaysia; azman2111@um.edu.my (A.M.); smzain@um.edu.my (S.B.M.Z.)

³ Department of Chemistry Education, UIN Sunan Gunung Djati, Bandung 40614, Indonesia

* Correspondence: atiek.noviyanti@unpad.ac.id (A.R.N.); ferli@uinsgd.ac.id (F.S.I.)

Abstract: The demand for synthetic bone grafts has increased in recent years. Hydroxyapatite (HA) is one of the highly suitable candidates as a bone graft material due to its excellent biocompatibility and high osteoconductive properties with low toxicity. HA has disadvantageous mechanical strength showing relatively fragile and brittle behavior due to its high hygroscopic properties. This leads to improper mechanical properties for such grafting applications. Therefore, HA should be combined with another material with similar biocompatibility and high hardness, such as SiO₂. In this work, HA/SiO₂ (HAS) composite material was prepared via a hydrothermal method to obtain the high purities of HA with a particle size of approximately 35 nm and around 50% crystallinity. It was found that the addition of SiO₂ stimulated the composite system by forming an orthosilicic acid complex that can reduce the overall solution's pH, thus contributing to the integrity and stability of the HAS composite. Therefore, higher SiO₂ contents in the HAS composite can enhance its mechanical stability when immersed in simulated body fluid (SBF). Our work demonstrated that HAS can highly improve HA material's hardness and mechanical stability under immersion of SBF. The Vickers test showed that the 0.05 GPa hardness in 10% SiO₂ increased to 0.35 GPa hardness with the addition of 20% SiO₂. The crystal structures of HAS were analyzed using X-ray diffraction, and the morphology of the HAS composites was observed under electron microscopy.

Keywords: hydroxyapatite-silica composite; hydrothermal method; simulated body fluid; highly stable mechanical properties



Citation: Noviyanti, A.R.; Juliandri, J.; Ernawati, E.E.; Haryono, H.; Solihudin, S.; Dwiyantri, D.; Ma'amor, A.; Irwansyah, F.S.; Zain, S.B.M. Hydrothermally Synthesized Hydroxyapatite-Silica Composites with Enhanced Mechanical Properties for Bone Graft Applications. *Chemistry* **2023**, *5*, 1645–1655. <https://doi.org/10.3390/chemistry5030113>

Academic Editors: Giulia Neri, Enza Fazio and Carmelo Corsaro

Received: 17 June 2023

Revised: 21 July 2023

Accepted: 24 July 2023

Published: 28 July 2023



Copyright: © 2023 by the authors. Licensee MDPI, Basel, Switzerland. This article is an open access article distributed under the terms and conditions of the Creative Commons Attribution (CC BY) license (<https://creativecommons.org/licenses/by/4.0/>).

1. Introduction

Recently, demands for bone and tooth grafts have surged dramatically [1,2]. Experts utilize autografts (bone implantations extracted from the patient's own body) to substitute the bone. Autografts involve taking bone tissue from the patient's body and are associated with significant drawbacks. These include the limited availability of donor tissue, high cost, and the potential risk of disease transmission. Consequently, exploring alternative materials that can address these challenges is crucial. One alternative is using synthetically prepared materials with properties similar to autografts, such as bio-ceramics, for bone grafting. Bio-ceramics have emerged as promising candidates for bone grafts due to their favorable characteristics. They exhibit high biocompatibility, meaning they are well-tolerated by the body without eliciting adverse reactions. It is essential for promoting healing and ensuring successful graft integration with the host tissue. Additionally, bio-ceramics possess osteoconductivity, providing a supportive scaffold for new bone formation

and enabling the regeneration of damaged or lost bone tissue. This property is crucial for restoring the structural integrity and function of the affected area. Furthermore, bio-ceramics demonstrate low toxicity, ensuring they do not introduce harmful substances into the body. In biomedical applications, minimizing the potential complications and adverse effects on patient health is paramount. By harnessing the advantageous properties of bio-ceramics, researchers and clinicians can overcome the limitations associated with autografts. Bio-ceramics offer a synthetic solution that can be reliably manufactured, readily available, and cost-effective compared to autografts. Their use as bone graft materials presents a viable alternative that can effectively address the challenges posed by autografts and enhance the success and accessibility of bone grafting procedures [3].

Hydroxyapatite (HA) is one example of a highly versatile bio-ceramic with a general formula of $\text{Ca}_{10}(\text{PO}_4)_6(\text{OH})_2$ and a Ca/P ratio of 1.67 [4]. HA has at least 65% of the components similarly found in the human bone and teeth structure. HA methods, including gel-casting foams, polymeric sponges, freeze-drying, tape casting, and salt leaching, have been reported to improve biocompatibility with human bone tissue [5]. Hydroxyapatite is valuable in the medical field, particularly as a bone and cartilage repair material, thanks to its outstanding biocompatibility and osteoconductive characteristics [6]. Despite the high biocompatibility [7], HA has disadvantageous mechanical strength showing relatively fragile and brittle behavior due to high hygroscopic properties. HA possesses hydroxyl groups that can readily absorb water from the ambiance. One method of modifying HA is through Ca ionic substitution. However, this method has some drawbacks, including rapid ion release. It can occur if ions are adsorbed or mixed within biomaterials without passing through the crystal lattice, which can be toxic to the surrounding tissue [7,8]. Therefore, HA should be combined with another material to accommodate these drawbacks [9].

The investigation involved evaluating the effectiveness of strongly alkaline solutions in processing medicinal ceramic powders and observing alterations in their phase composition and surface morphology. Two ceramic powders, alumina, and zirconia, underwent treatment with two etchant mixtures, resulting in minimal alterations. However, the surface exhibited modifications by depositing a Ca-deficient hydroxyapatite layer. In the zirconia case, the deposited layer displayed a nearly continuous, fine film that effectively covered the ceramic surface. Analysis of the FTIR spectra revealed a significant shift in the ZrO_2 band from 486 cm^{-1} to around 501 cm^{-1} , while the CDH band did not experience any shift. This indicates an evident interaction between CDH and the modified ZrO_2 surface, leading to improved “wetting” properties due to the alkaline treatment. Therefore, the treated zirconia surface shows promise as a potential bioceramic material for medical applications such as prosthetics [10].

An effective method to transport Ca-deficient hydroxyapatite to the targeted region is through a nanocomposite formulation, where the primary constituent of the nanocomposite is a clay mineral. Clay minerals are already extensively utilized in pharmaceutical applications as active agents with therapeutic properties or excipients. These minerals offer various advantageous characteristics, including surface reactivity (such as cation exchange, swelling, and absorption), solubility, a significant specific surface area, and non-toxicity for human use [11]. In the process of creating dental composites, the treatment of inorganic particles with silane is employed to enhance their chemical interaction with the organic matrix, potentially leading to improved mechanical properties of the composite. Despite limited information on the impact of this process on the ion release capabilities of bioactive composites containing different calcium phosphate complexes, its influence on enamel remineralization still needs to be explored. The silanization of particles would not affect the remineralization potential of the composite [12].

Silica (SiO_2) is one of the suitable candidates for a composite with HA. SiO_2 has better mechanical properties with 6–7 Mohs’ hardness, while HA shows a hardness of around 5 [13]. Moreover, SiO_2 has similar biocompatibility with a low thermal expansion coefficient of $\sim 10^{-7}\text{ K}^{-1}$, which can be quite beneficial for maintaining the structure of the HA/ SiO_2 (HAS) composite under high temperatures. HAS can be prepared by various

methods, i.e., sonochemistry, sol-gel, and hydrothermal methods [14]. Hydrothermal synthesis offers a relatively straightforward and easily scalable method, which is more environmentally friendly than other nanotechnology production techniques. This approach allows for precise control and high repeatability in achieving desired microstructures. Hydrothermal synthesis enables the alteration of nanoparticles' surface properties by appropriately selecting surface-coating agents, transforming them from hydrophilic to hydrophobic [15]. The visibility of pH sensitivity will be enhanced when observing the effect within a narrow optimal pH range, minimizing the difference between the values [16]. Previously, a composite prepared through sonochemistry from an *onyx* crystal with an HA-to-SiO₂ ratio of 80:20 resulted in a crystal size of 30.57 nm with a *Vickers* hardness of 26.72 HV [17]. An HAS prepared for collagen scaffolding via the sol-gel method showed high stability in acidic conditions, yet the hardness was not investigated. In comparison, the preparation of HA via a hydrothermal method suggested a highly improved crystallite size of 35.28 nm with a purity of 99.5% [18].

In this study, we focused on examining the mechanical stability of a composite material called HA/SiO₂ (HAS) when immersed in simulated body fluid (SBF), first synthesizing hydroxyapatite (HA) to create the composite through a hydrothermal process. Silica dioxide (SiO₂) was also prepared using rice husk as the raw material. Subsequently, we combined the HA and SiO₂ using the hydrothermal method, forming the HA/SiO₂ composite, which exhibited improved stability and mechanical properties. This research is unique in that it explores the mechanical strength of the HAS composite when subjected to immersion in SBF. Before this study, the preparation of HAS through direct combination of its constituents using the hydrothermal method had not been reported. Therefore, our research contributes novel insights into the HA/SiO₂ composite synthesis.

Furthermore, our study found that the mechanical hardness of the composite was enhanced by incorporating 20% SiO₂. This result suggests that adding SiO₂ positively impacts the composite material's mechanical properties. The improved mechanical hardness holds promise for the potential application of HAS as a bone graft material in the future. Overall, our approach of synthesizing the HA/SiO₂ composite through the hydrothermal method, investigating its mechanical stability in SBF, and demonstrating the enhancement of mechanical hardness through SiO₂ addition offers valuable insights for developing and utilizing HAS in bone graft materials.

2. Materials and Methods

2.1. Materials

CaO (obtained from thermal treatment of chicken egg shells), ammonium dihydrogen phosphate (NH₄H₂PO₄ Sigma 99% CAS No. 7722-76-1, Burlington, MA, USA), silica (SiO₂) obtained from gasification of rice husk, and simulated body fluid (SBF).

2.2. Instrumentation

Oven Carbolite, XRD (PANalytical X'Pert PRO serial PW3040/X0, Malvern, UK), FTIR (PerkinElmer Spectrum 100, Waltham, MA, USA), SEM-EDS (Jeol Jsm-6360LA, Akishima, Japan), and micro-Vickers hardness tester (HMV-G21ST, Kawasaki-shi, Japan).

2.3. Procedure

2.3.1. Synthesis of HA

HA was prepared using the hydrothermal method [18]. Eggshells obtained from the chicken egg were cleansed from the contaminants and biological membranes using deionized water. The ball mill created smaller eggshell particles of ~100 mesh size. The crushed eggshells were calcined at 1000 °C for five hours to convert CaCO₃ into CaO as the precursor of HA synthesis. The obtained CaO was mixed with dihydrogen phosphate stoichiometrically with a Ca/P ratio of 1.67 in deionized water in a 100 mL autoclave. The mixture was heated at 230 °C for 48 h using hydrothermal synthesis. The prepared HA was

filtered before washing with deionized water until pH 7 to eliminate the NH_4OH from the side reaction. The washed white powder was dried at $110\text{ }^\circ\text{C}$ for two hours.

2.3.2. Preparation of SiO_2 from Rice Husk

A solution mixture of carbonized rice husk, sodium hydroxide, and deionized water was stirred with heating at $100\text{ }^\circ\text{C}$ for 150 min. The hot mixture was directly filtered to obtain the solid residue. The residue was settled at room temperature, and an aqueous HCl solution (1:1 *w/w*) was incrementally added to the residue until the pH reached 7. The white silica started to precipitate and collect. The silica powder was refiltered and washed before being dried in an oven at $110\text{ }^\circ\text{C}$ for two hours.

2.3.3. Preparation of HA/ SiO_2 (HAS) Composites

The synthesized HA was mixed with SiO_2 with various HA: SiO_2 ratios of 90:10 (HAS90), 85:15 (HAS85), and 80:20 (HAS80) using mechanical stirring in 60 mL deionized water. The mixture of HAS was put into an autoclave for hydrothermal preparation at $230\text{ }^\circ\text{C}$ for 48 h. The precipitate was filtered and washed with deionized water before drying at $110\text{ }^\circ\text{C}$ for two hours. The synthesis process for HAS composite is shown in Figure 1.

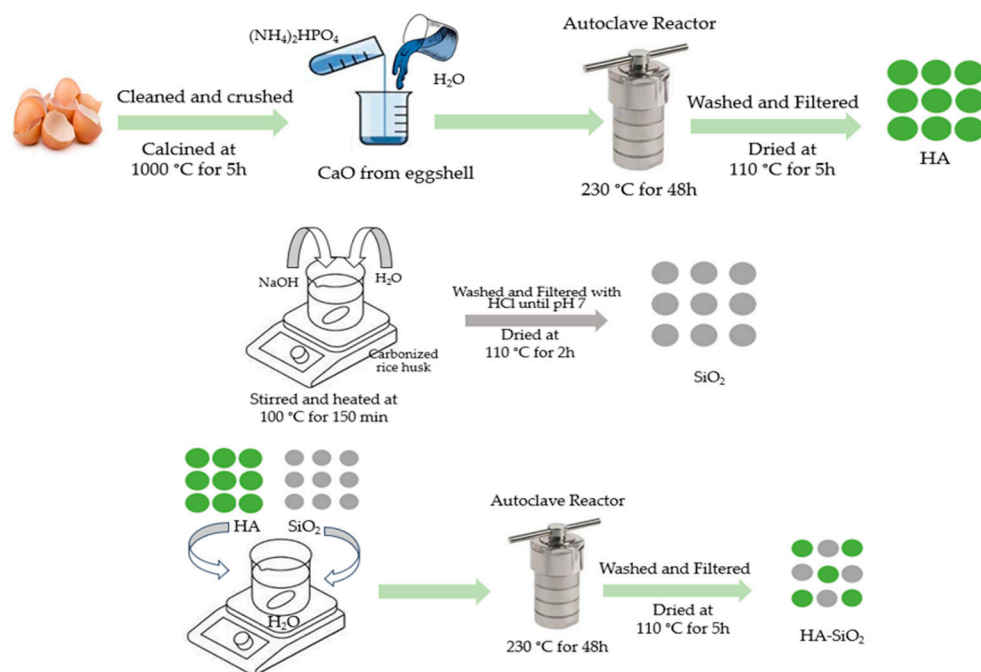


Figure 1. Synthesis of HA/ SiO_2 (HAS) composites by hydrothermal method.

2.3.4. Structural Investigation of HA/ SiO_2 (HAS) Composites

The crystal structure obtained was analyzed using X-ray diffraction (XRD, *Bruker D8 Advance*) with $\text{CuK}\alpha = 1.5311$ at the 2θ range of $20\text{--}90^\circ$. The morphology of HAS was observed under electron microscopy (SEM, *Jeol JSM-6360LA*) with a voltage of 20 kV at various magnifications of 500, 1000, and 4000, while the Fourier-transformed infrared spectra (FTIR) were collected using *Perkin Elmer Spectrum 100* at a wavenumber range of 4000 to 500 cm^{-1} . The HAS samples were pressed into pellets by mixing them with KBr salts.

2.3.5. Characterization of HAS Composites Mechanical Properties

The hardness of HAS samples was analyzed using a *micro Vickers hardness* test machine to obtain Vicker's hardness value. The HAS samples were pelleted to achieve a circular shape, while a load of 100 g was subjected to the HAS pellets for 10 s.

2.3.6. In Vitro Test for Biodegradation of HAS Composite Materials

The simulation of the biodegradation of HAS was conducted to observe the decay rate over the mass loss of the HAS samples by immersing the HAS pellets in simulated body fluid (SBF). SBF ion content concentrations are similar to that in blood plasma [19]. The pellets of HAS were immersed in SBF with a pH of 7.67 for three days at a temperature of 37 °C. After three days of immersion, the pHs of the SBF solutions were measured while HAS pellets were washed with deionized water and dried at 70 °C for 2 h. The mass of pellets was weighed until constant, and the mass loss was calculated compared to the initial mass of the HA pellets.

3. Results

HA has a hexagonal structure with phosphates coordinated to the calcium metal center. The base structure of HA is calcium apatite with a formula of $\text{Ca}_5(\text{PO}_4)_3(\text{OH})$, frequently written as $\text{Ca}_{10}(\text{PO}_4)_6(\text{OH})_2$, indicating its double molecule in one crystal structure, as shown in Figure 2. With the space group of $P63/m$, HA has a lattice parameter of $a = b = 9.4321 \text{ \AA}$ and $c = 6.881 \text{ \AA}$ [20]. Silica has a tetrahedral structure with SiO_4 clusters connecting each other. It has a lattice parameter of $a = 4.973 \text{ \AA}$, $b = 6.923 \text{ \AA}$, and $c = 1.392 \text{ \AA}$ based on JCPDS. Silica here frequently appears as a more amorphous phase t , but the diffraction pattern usually only shows one or two main peaks.

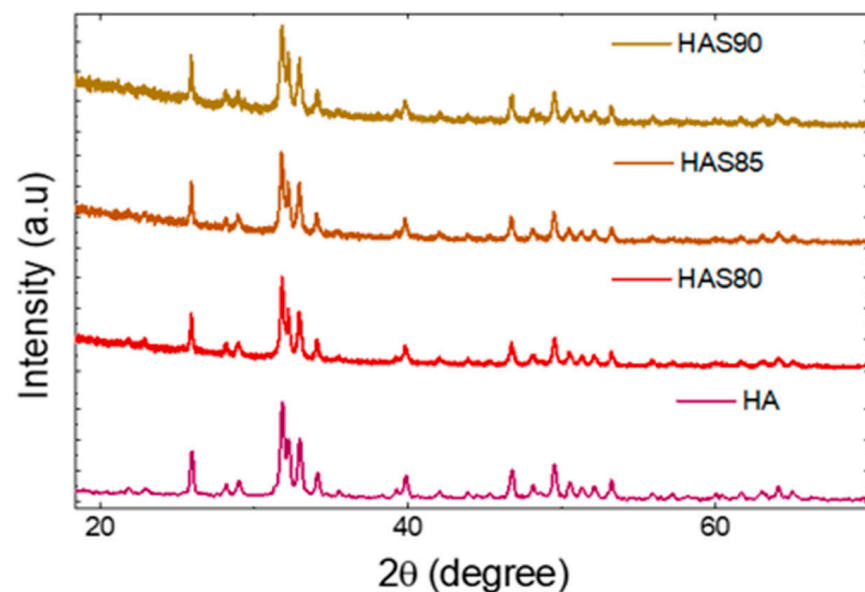


Figure 2. XRD patterns of HAS with different ratios of HA:SiO₂.

The crystallite size was determined through Equation (1).

$$D = \frac{k\lambda}{\beta \cos \theta} \quad (1)$$

where D is the crystallite size (nm), k is the crystal shape factor (0.9–1.0), λ is the X-ray wavelength (0.15406 nm), β = Full Width at Half Maximum (FWHM) (rad), and θ = diffraction angle (deg). In comparison, the crystallinity can be calculated from Equation (2).

$$X_c = \frac{A_\theta}{A_{total}} \times 100\% \quad (2)$$

where X_c is the crystallinity (%), A_θ is the area intensity of the crystalline contribution at which the main pattern is located, $2\theta = 31.78^\circ$, d_{hkl} (211). At the same time, A_{total} is the total area intensity from the contribution of crystalline and amorphous regions.

HA has the main peak at 2θ of 31.78° (see Figure 1); from this peak, the crystallinity of HAS can be calculated as listed in Table 1. Silica, on the other hand, is more amorphous compared to HA. Therefore, adding silica to HA can reduce the crystallinity by up to 50%. Interestingly, the crystallinity does not follow the trend of SiO_2 contents yet has the lowest value of 48.6% for HAS85 [21]. It is probably due to a micromolecular interaction between HA and SiO_2 which results in the partial substitution of $-\text{PO}_4$ groups in HA with the presence of an SiO_4 cluster as the following reaction [22]:



Table 1. The crystallinity of HAS composites.

Materials	Crystallite Size (nm)	Crystallinity (%)
HA [9]	35.28	99.5
HAS90	34.82	50.5
HAS85	35.80	48.6
HAS80	34.21	53.1

The lattice parameters of HAS is listed on Table 2. The composites show a slight reduction at the a, b-, and c-directions compared to standard HA, and the increase of SiO_2 content indicates that distributions of SiO_2 throughout the HA particles slightly distorted the hexagonal structure of HA. This change has no significant effect on the distortion. Therefore, the base crystal structure of HA remains stable in the composite. At the same time, a slight decrease in lattice parameter is reasonable since SiO_2 has an amorphous phase and is within the higher contents.

Table 2. Lattice parameters of HAS composites.

Materials	Structure	Space Group	$a = b$ (Å)	c (Å)	Intensity Ratio (27.2 to 31.78°)	Density ($\text{g}\cdot\text{cm}^{-3}$)
HA ICSD 96-900-2215	Hexagonal	$P 6_3/m$	9.4390	6.8860		3.14
HAS90			9.4171	6.8753	0.77	3.16
HAS85			9.4168	6.8751	0.64	3.16
HAS80			9.4142	6.8749	0.49	3.16

FTIR analysis was deployed to investigate further functional group interactions between HA and SiO_2 in the composite, as seen in Figure 3 and listed in Table 3. The FTIR spectra show the main peak of the phosphate group at $\sim 560\text{ cm}^{-1}$, which indicates the presence of HA, while OH^- peaks at 630 and 3560 cm^{-1} suggest the presence of both HA and SiO_2 , respectively. However, the main peaks of SiO_2 , indicated by Si–OH and O–Si–O, are observed at the wavenumbers of approximately 800 and 475 cm^{-1} , respectively [22,23]. The presence of all contributing peaks from HA and SiO_2 suggests that an HAS composite was successfully prepared by the hydrothermal method.

The SEM micrograph shows HAS composite morphology (Figure 4a). At the magnification of $4000\times$, HAS with higher contents of SiO_2 (20 wt.%) suggests more agglomerated particles, with homogeneous distributions showing a particle median of 650 nm (Figure 4b). The HAS composites with lower SiO_2 contents (15 and 10 wt.%) denote median particle sizes of ~ 500 and 600 nm, respectively. Interestingly, the HAS showed an optimum trend as $\text{HAS80} > \text{HAS90} > \text{HAS85}$. The contribution of amorphous SiO_2 in the composites can enhance the agglomeration of HAS particles, probably due to stronger hydrogen interactions between Si–OH from SiO_4 tetrahedral sites and Ca–OH from HA sites as increasing SiO_2 content. However, the absolute value of the HAS particle size from *ImageJ* analysis might differ from the actual size. Furthermore, we also conducted particle size analysis (PSA) using a PSA analyzer, as seen in Table 4. The results suggested that the particle size of HAS

follows this trend: HAS90 (1660.1 nm), HAS80 (1640.1 nm), and HAS85 (1462.0 nm), which consistently follows the trend obtained from *ImageJ* analysis. Data regarding the value of the mean, mode, median, standard deviation, and polydispersity index (PI) are shown in Table 4.

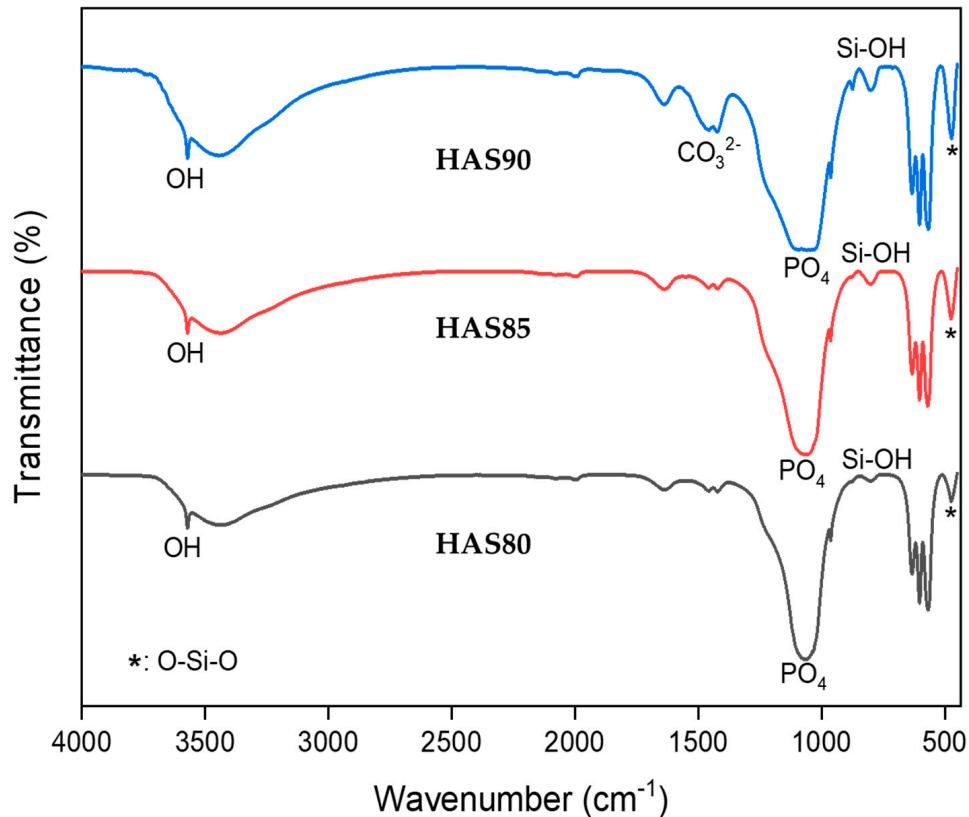


Figure 3. FTIR spectra of HAS with different ratios of HA:SiO₂.

Table 3. Functional group assignment of HAS materials.

Functional Groups	Wavenumber (cm ⁻¹)			
	Reference [18]	HAS90	HAS85	HAS80
PO ₄ ³⁻	564	567.00	570.96	566.92
	605	602.95	602.95	602.72
	964	963.01	963.02	962.84
	1062	1063.90	1061.59	1063.16
	2002	2002.94	2002.85	2002.84
OH	631	632.27	632.05	632.49
	3568	3571.72	3571.54	3571.84
CO ₃ ²⁻	1420	1421.95	1421.91	1423.14
Si-OH	799	802.49	796.74	799.11
O-Si-O	475	474.23	474.97	475.64

Table 4. Particle size analysis statistics of HAS with different SiO₂ contents.

Sample	Measurement Parameters				
	Mean (nm)	Mode (nm)	Median (nm)	Standard Deviation	PI
HAS 80 20	1631.0	1746.5	1640.0	190.5	1.250
HAS 85 15	1459.1	1643.7	1462.0	282.2	1.438
HAS 90 10	1649.4	1748	1660.1	182.1	0.807

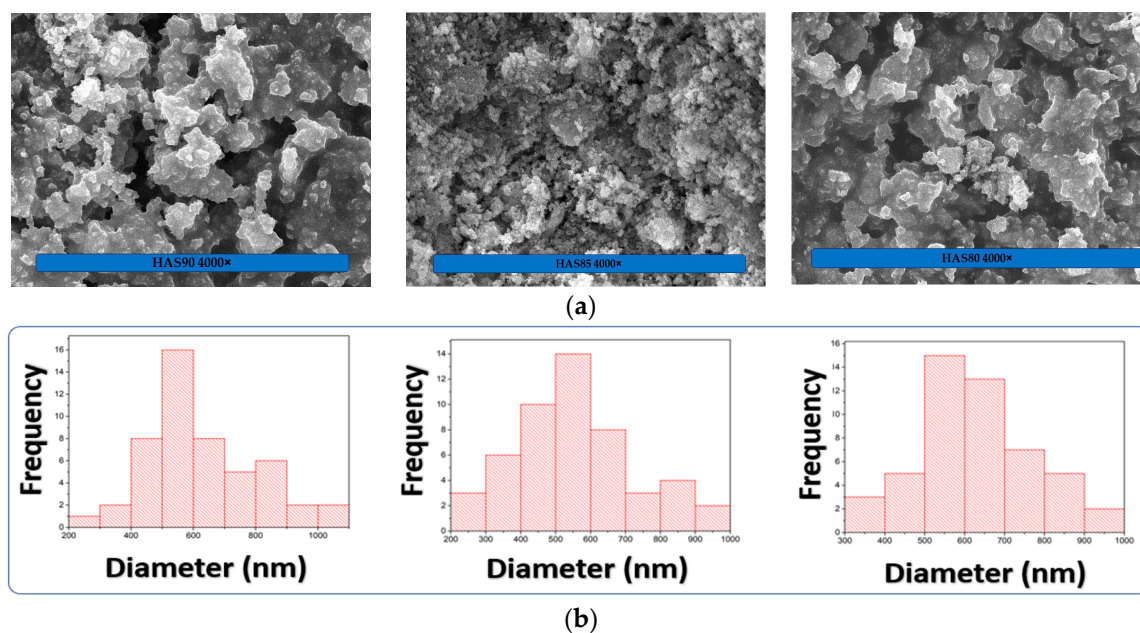


Figure 4. (a) SEM micrographs of HAS composite materials with different HA/SiO₂ ratios showing a porous structure of HAS with larger content of SiO₂ (HAS80). (b) Particle size distribution was obtained from micrograph analysis using ImageJ software.

A lower value generally indicates a narrower and more uniform particle size distribution in the context of PI values. A higher PI value in particle size analysis indicates a wider and more heterogeneous particle size distribution, meaning a greater range of particle sizes is present in the sample. In such cases, the sample contains a greater range of particle sizes, with some particles being significantly larger or smaller than the average size. This can result in a less uniform distribution, with both large and small particles in the sample. A sample with a PI value close to 0.1 would have a very narrow distribution of particle sizes, where most particles are very similar. On the other hand, a sample with a PI value close to 0.9 would have a wide distribution, indicating a significant variation in particle sizes. The PI value is a valuable parameter in particle size analysis as it provides insights into the homogeneity or heterogeneity of particle size distribution. It is crucial in various applications, such as material synthesis, drug delivery systems, and product quality control. A lower PI value is generally preferred for a more consistent and controlled particle size distribution [24]. Therefore, among the PI values we had (0.8, 1.4, and 1.25), the PI value of 0.8 (HAS 90) is considered the best to have a more uniform particle size distribution.

To test the robustness of HA-based composites for practical application, we immersed the HAS materials in simulated body fluid (SBF) for three days, and the pH change and its mass loss were monitored during the process. After three days of immersion, we found that the pH of HAS90 increased significantly from its SBF baseline of pH (7.6), as seen in Figure 5A, yet showed no appreciable difference from the HA-based standard. The significant increase of HAS can be attributed to the partial dissolution of HA creating OH⁻ anions during the immersion, as shown in the chemical equation below [25]. The degradation rate of HAp-based materials increased logarithmically as a function of time [26]. The general dissolution of HA in water can be written as the equilibrium reaction below:



The water has a pH close to the pH of SBF, which suggests that the immersion of HAS in SBF fluid can act similarly as described in the chemical equation above [25]. The HAS material is immersed in the SBF fluid. It is expected to behave similarly to how it would behave in water due to the similarity in their pH levels. In other words, the properties and reactions of HAS in SBF might be comparable to those in water because the pH

conditions are comparable. The pH level is an important factor to consider in the behavior of HAS in SBF. Since the pH of the SBF is similar to that of water, it may provide a suitable environment for evaluating how the HAS material interacts and reacts with the fluid, using SBF as a simulation of the body's natural environment to assess the biocompatibility and bioactivity of materials intended for medical or biological applications, especially those related to bone and tissue regeneration. The similar pH levels between water and SBF make the immersion in SBF a relevant and informative experiment to understand the potential response of HAS in a physiological-like environment.

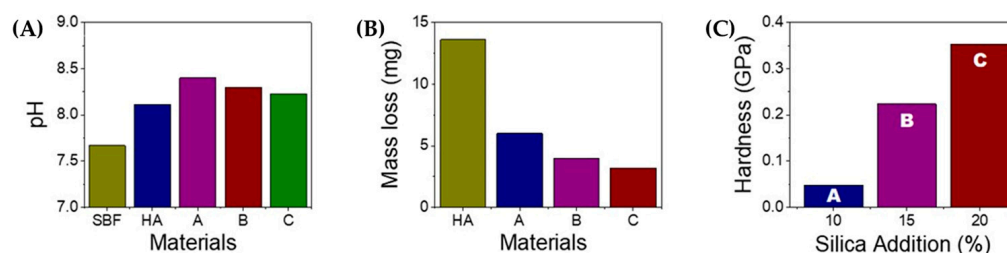


Figure 5. Physical properties of HAS composite materials (A = HAS90, B = HAS85, C = HAS80). (A) pH of HAS materials after immersion in SBF for three days. (B) Mechanical stability of HAS material during immersion in SBF. (C) Mechanical strength of HAS with various amounts of silica added.

Interestingly, the addition of silica can reduce the pH. With the higher content of SiO_2 , the pH returns closer to that of its original base materials, probably due to the formation of orthosilicic acid (H_4SiO_4) from the hydrolysis of SiO_2 . SiO_2 can act as a buffer to stabilize the basic condition of HAS. In an aqueous environment, SiO_2 can dissociate to $\text{SiO}_4^{4-} + 4\text{H}^+$. The generated protons will subsequently neutralize the hydroxyl ions [15]. The generation of orthosilicic is also known to give biological and potential therapeutic effects [16], which can be very beneficial for applying HAS-based materials such as bone grafts. This trend is also followed by its mass loss of HA, which shows highly stable HAS with a higher content of SiO_2 . Silica has similar water absorptivity of water with HA. The porous structure of silica can contain more water than HA. Thus, silica can stabilize the overall composite structure in HAS.

The HAS with a higher content of SiO_2 shows less mass loss (Figure 5B), consistent with the enhanced hardness (Figure 5C). The addition of silica is proven to increase the hardness more than three times higher than that of the low content of SiO_2 due to a contribution from the intrinsic hardness of SiO_2 . Therefore, HAS with high content of SiO_2 can be applicable for bone grafts.

4. Conclusions

The hydrothermal method successfully prepared the HA/ SiO_2 (HAS) composites, resulting in a crystallite size of approximately ~35 nm and around ~50% crystallinity. The addition of SiO_2 stimulated the composite system by forming an orthosilicic acid complex, which reduced the overall solution's pH. SiO_4^- species acted as a conjugated base, creating a buffering effect within the mixture, thus contributing to the integrity and stability of the HAS composite and incorporating higher SiO_2 contents in the HAS composite enhanced mechanical stability when immersed in SBF. It was evidenced by increased mechanical hardness, as measured by the Vickers test, from 0.05 GPa to 0.35 GPa with the addition of 20% SiO_2 . These results indicate that the inclusion of SiO_2 positively influenced the mechanical properties of the composite material, rendering it more resistant and robust. Based on the improved stability and mechanical properties observed in the HAS composites, they hold great potential as bone graft material for future applications. The stability of the composite, combined with the increased mechanical hardness, makes it a promising candidate for use in bone grafting procedures. The excellent properties of the HAS composites make them a valuable option to consider in developing advanced bone grafting materials.

Author Contributions: A.R.N. conducted Conceptualization, Investigation, Visualization, Funding Acquisition, Writing—Original Draft, Writing—Review and Editing; D.D. conducted Formal Analysis, Writing—Review, and Editing; J.J., E.E.E., H.H., S.S., F.S.I., A.M. and S.B.M.Z. Writing—Review and Editing. All authors have read and agreed to the published version of the manuscript.

Funding: This work was supported by Universitas Padjadjaran through Riset Kompetensi Dosen Unpad Grant No. 2203/UN6.3.1/PT.00/2022. Academic Leadership Grants Unpad No. 1549/UN6.3.1/PT.00.2023 also partially supported this work.

Data Availability Statement: The authors declare no supplementary data is available.

Acknowledgments: The authors deliver the gratitude to Yoga Trianzar Malik for fruitful discussion on this work and to Rika Yunisya Dwi Pratiwi, who assisted in collecting experimental data.

Conflicts of Interest: The authors declare no conflict of interest.

References

1. Li, T.-T.; Ling, L.; Lin, M.-C.; Peng, H.-K.; Ren, H.-T.; Lou, C.-W.; Lin, J.-H. Recent advances in multifunctional hydroxyapatite coating by electrochemical deposition. *J. Mater. Sci.* **2020**, *55*, 6352–6374. [[CrossRef](#)]
2. Kim, S.; Park, C.B. Bio-Inspired Synthesis of Minerals for Energy, Environment, and Medicinal Applications. *Adv. Funct. Mater.* **2012**, *23*, 10–25. [[CrossRef](#)]
3. Daulbayev, C.; Sultanov, F.; Korobeinyk, A.V.; Yeleuov, M.; Taurbekov, A.; Bakbolat, B.; Umirzakov, A.; Baimenov, A.; Daulbayev, O. Effect of graphene oxide/hydroxyapatite nanocomposite on osteogenic differentiation and antimicrobial activity. *Surf. Interfaces* **2022**, *28*, 101683. [[CrossRef](#)]
4. Panda, S.; Biswas, C.K.; Paul, S. A comprehensive review on the preparation and application of calcium hydroxyapatite: A special focus on atomic doping methods for bone tissue engineering. *Ceram. Int.* **2021**, *47*, 28122–28144. [[CrossRef](#)]
5. Chen, Q.; Zou, B.; Lai, Q.; Wang, Y.; Xue, R.; Xing, H.; Fu, X.; Huang, C.; Yao, P. A study on biosafety of HAP ceramic prepared by SLA-3D printing technology directly. *J. Mech. Behav. Biomed. Mater.* **2019**, *98*, 327–335. [[CrossRef](#)]
6. Chen, Q.; Zou, B.; Lai, Q.; Zhao, Y.; Zhu, K. Influence of irradiation parameters on the curing and interfacial tensile strength of HAP printed part fabricated by SLA-3D printing. *J. Eur. Ceram. Soc.* **2022**, *42*, 6721–6732. [[CrossRef](#)]
7. Wopenka, B.; Pasteris, J.D. A mineralogical perspective on the apatite in bone. *Mater. Sci. Eng. C* **2005**, *25*, 131–143. [[CrossRef](#)]
8. Wang, L.; Nancollas, G.H. Calcium Orthophosphates: Crystallization and Dissolution. *Chem. Rev.* **2008**, *108*, 4628–4669. [[CrossRef](#)]
9. Zakharova, O.; Gusev, A.; Chuprunov, K.; Yudin, A.; Kuznetsov, D. Cytotoxic Effects of Granulated Hydroxyapatite with Various Particle Size Distribution. *IOP Conf. Ser. Mater. Sci. Eng.* **2020**, *731*, 012020. [[CrossRef](#)]
10. Nakonieczny, D.S.; Martynková, G.S.; Hundáková, M.; Kratošová, G.; Holešová, S.; Kupková, J.; Pazourková, L.; Majewska, J. Alkali-Treated Alumina and Zirconia Powders Decorated with Hydroxyapatite for Prospective Biomedical Applications. *Materials* **2022**, *15*, 1390. [[CrossRef](#)] [[PubMed](#)]
11. Pazourková, L.; Reli, M.; Hundáková, M.; Pazdziora, E.; Predoi, D.; Simha, M.G.; Lafdi, K. Study of the structure and antimicrobial activity of Ca-deficient ceramics on chlorhexidine nanoclay substrate. *Materials* **2019**, *12*, 2996. [[CrossRef](#)] [[PubMed](#)]
12. Reis, D.P.; Noronha, F.J.D.; Rossi, A.L.; Neves, d.E.A.; Portela, M.B.; Silva, d.E.M. Remineralizing potential of dental composites containing silanized silica-hydroxyapatite (Si-HAp) nanoporous particles charged with sodium fluoride (NaF). *J. Dent.* **2019**, *90*, 103211. [[CrossRef](#)] [[PubMed](#)]
13. Tabor, D. Mohs's Hardness Scale—A Physical Interpretation. *Proc. Phys. Soc. Sect. B* **1954**, *67*, 249–257. [[CrossRef](#)]
14. Pai, S.; Kini, S.M.; Selvaraj, R.; Pugazhendhi, A. A review on the synthesis of hydroxyapatite, its composites and adsorptive removal of pollutants from wastewater. *J. Water Process Eng.* **2020**, *38*, 101574. [[CrossRef](#)]
15. Irwansyah, F.S.; Noviyanti, A.R.; Eddy, D.R.; Risdiana, R. Green Template-Mediated Synthesis of Biowaste Nano-Hydroxyapatite: A Systematic Literature Review. *Molecules* **2022**, *27*, 5586. [[CrossRef](#)]
16. Irwansyah, F.S.; Yusuf, A.; Eddy, D.R.; Risdiana, R.; Noviyanti, A.R. Effect of Sensitive pH on Hydroxyapatite Properties Synthesized from Chicken Eggshell. *Indones. J. Chem.* **2022**, *22*, 1418–1426. [[CrossRef](#)]
17. Hartatiek; Reri, D.; Hartanto, Y.A.; Hidayat, N.; Yudyanto; Utomo, J. Sunaryono the Effect of Sonication Duration on the Characteristics of Nano Hydroxyapatite-Silica (nHAp/SiO₂) Composite and its Mechanical Properties. *J. Phys. Conf. Ser.* **2018**, *1093*, 012019. [[CrossRef](#)]
18. Noviyanti, A.R.; Akbar, N.; Deawati, Y.; Ernawati, E.E.; Malik, Y.T.; Fauzia, R.P. Risdiana A novel hydrothermal synthesis of nanohydroxyapatite from eggshell-calcium-oxide precursors. *Heliyon* **2020**, *6*, e03655. [[CrossRef](#)] [[PubMed](#)]
19. Har, I.N.P.; Irzaman, N.P. Crystallinity and electrical properties of silicon dioxide (SiO₂) from rice straw. *AIPC* **2019**, *2202*, 020028. [[CrossRef](#)]
20. Palard, M.; Champion, E.; Foucaud, S. Synthesis of silicated hydroxyapatite Ca₁₀(PO₄)_{6–x}(SiO₄)_x(OH)_{2–x}. *J. Solid State Chem.* **2008**, *181*, 1950–1960. [[CrossRef](#)]
21. Moreno-Perez, B.; Matamoros-Veloz, Z.; Rendon-Angeles, J.C.; Yanagisawa, K.; Onda, A.; Pérez-Terrazas, J.E.; Mejia-Martínez, E.E.; Díaz, O.B.; Rodríguez-Reyes, M. Synthesis of silicon-substituted hydroxyapatite using hydrothermal process. *Boletín De La Soc. Española Cerámica Vidr.* **2020**, *59*, 50–64. [[CrossRef](#)]

22. Wang, H. Hydroxyapatite Degradation and Biocompatibility. 2004. Available online: https://www.researchgate.net/publication/252511979_Hydroxyapatite_degradation_and_biocompatibility (accessed on 28 March 2023).
23. You, B.C.; Meng, C.E.; Nasir, N.F.M.; Tarmizi, E.Z.M.; Fhan, K.S.; Kheng, E.S.; Majid, M.S.A.; Jamir, M.R.M. Dielectric and biodegradation properties of biodegradable nano-hydroxyapatite/starch bone scaffold. *J. Mater. Res. Technol.* **2022**, *18*, 3215–3226. [[CrossRef](#)]
24. Mudalige, T.; Qu, H.; Van Haute, D.; Ansar, S.M.; Paredes, A.; Ingle, T. Characterization of Nanomaterials. In *Micro and Nano Technologies*; Elsevier: Amsterdam, The Netherlands, 2019; pp. 313–353. [[CrossRef](#)]
25. Demianenko, E.; Ilchenko, M.; Grebenyuk, A.; Lobanov, V. A theoretical study on orthosilicic acid dissociation in water clusters. *Chem. Phys. Lett.* **2011**, *515*, 274–277. [[CrossRef](#)]
26. Jurkić, L.M.; Ceganec, I.; Pavelić, S.K.; Pavelić, K. Biological and therapeutic effects of ortho-silicic acid and some ortho-silicic acid-releasing compounds: New perspectives for therapy. *Nutr. Metab.* **2013**, *10*, 1–12. [[CrossRef](#)] [[PubMed](#)]

Disclaimer/Publisher's Note: The statements, opinions and data contained in all publications are solely those of the individual author(s) and contributor(s) and not of MDPI and/or the editor(s). MDPI and/or the editor(s) disclaim responsibility for any injury to people or property resulting from any ideas, methods, instructions or products referred to in the content.